Journal of The Electrochemical Society, 2022 **169** 044527
1945-7111/2022/169(4)/044527/8/$40.00 © 2022 The Electrochemical Society ("ECS"). Published on behalf of ECS by IOP Publishing Limited

Promoting CO_2 Release from CO_3^{2-}-Containing Solvents during Water Electrolysis for Direct Air Capture

Xin Gao,[1,2] Ayokunle Omosebi,[1,z] Roger Perrone,[1] and Kunlei Liu[1,2,z]

[1]*University of Kentucky Center for Applied Energy Research, Lexington, Kentucky 40511, United States of America*
[2]*Department of Mechanical Engineering, University of Kentucky, Lexington, Kentucky 40506, United States of America*

The pH swings from water electrolysis are leveraged to condition OH^--based facile CO_2 capture solvents using an electrochemical flow cell for direct air capture (DAC). Besides demonstrating the DAC using a membrane contactor, promoting CO_2 release from a CO_3^{2-} solution at the anode is specifically studied by adjusting the volumetric flow rate, anode chamber volume, residence time, and K_2CO_3 concentration. Through case-by-case comparisons coupled with modeled results, increasing current, reducing volumetric flow rate, and/or reducing CO_3^{2-} concentration are the effective methods to promote CO_2 release from a CO_3^{2-}-containing solvent, whereas enlarging the anode chamber volume poses a minor effect. Moreover, the discrepancies between the experimental and modeled results may be caused by H^+ crossover rather than K^+ transport through the Nafion membrane during water electrolysis based upon the total alkalinity measurements for the K_2CO_3 solutions gleaned from the anode. It is believed that such results will provide guidance to design and operate an electrochemical flow cell for electrochemistry-assisted DAC and point source CO_2 capture.
 [DOI: 10.1149/1945-7111/ac5fef]

Manuscript submitted December 20, 2021; revised manuscript received March 14, 2022. Published April 27, 2022.

Supplementary material for this article is available online

The goal of the Paris Climate Agreement is to limit the increase in the global average temperature to 2 °C above pre-industrial levels in this century.[1] To meet this requirement, capturing CO_2 is essential for point sources, e.g., fossil fuel power generation plants, oil refineries, cement and steel manufacturers, and open sources like air. A common CO_2 capture practice employs a chemical-thermal process, where a low-volatility amine solvent captures CO_2 in an absorber, followed by liberating the captured CO_2 and refreshing the amine solvent at 100 °C–120 °C in a stripper.[2–4] While such a process is adequate for high concentration CO_2 capture from flue gas, e.g., 12–15 vol% CO_2 from coal-fired plants and 25 vol% from cement and steel production,[2,5,6] directly capturing 0.04 vol% CO_2 from air stresses the capture process with the implication that new approaches with greater capture capacities and rates are preferred for CO_2 capture at low levels.[7–9] In this work, an alternative approach assisted by an electrochemical flow cell is studied, leveraging the pH swings resulting from water electrolysis to recondition OH^--based facile CO_2 capture solvents in a membrane-electrochemical carbon capture-enrichment process for low concentration CO_2 capture.[10] Such an electrochemistry-assisted carbon capture process will possess the key merits of no nitrosamine formation, no heating requirement, and excellent carbon capture rate in comparison to the conventional amine-thermal process.

A schematic of the membrane-electrochemical CO_2 capture-enrichment process is shown in Fig. 1a, similar to the concept that has been proposed in Ref. 11. CO_2 in air reacts with dissolved KOH in the membrane contractor, forming K_2CO_3 via $CO_2 + 2KOH \leftrightarrow K_2CO_3 + H_2O$ to attain a fast carbon capture rate, as demonstrated in a case study in Fig. 6. To retain the fast carbon capture rate, the K_2CO_3 solvent is needed to be regenerated to KOH in the electrochemical flow cell, which is predominantly driven by the pH swings from water electrolysis, as depicted in Figs. 1b and 1c. Due to producing O_2 by consuming OH^- via $4OH^- \rightarrow O_2\uparrow + 2H_2O + 4e^-$ in the anode chamber, CO_3^{2-} is transformed to CO_2 through $CO_3^{2-} + H_2O \leftrightarrow HCO_3^- + OH^-$ followed by $HCO_3^- \leftrightarrow CO_2\uparrow + OH^-$. Concurrently, to balance the negative OH^- ionic charge coming from $2H_2O + 2e^- \rightarrow H_2\uparrow + 2OH^-$, the positive K^+ ionic charge migrates across the cation exchange membrane to the cathode chamber, thereafter, producing KOH that will be used to capture CO_2 in the membrane contactor. Overall, releasing CO_2 from CO_3^{2-} solution is the consequential step following the O_2 evolution at the anode, and its effectiveness relies primarily on reducing the OH^- concentration in the anode chamber.

Unlike thermal and H_2 gas assisted solvent regeneration approaches,[4,12] the present cell architecture in Fig. 1 (i.e., two metal plate electrodes separated by a cation exchange membrane) will release CO_2 while producing O_2 at the anode. Under such a competing scenario, a high yield of CO_2 will be preferred if purified CO_2 is needed for beneficial uses, e.g., molten carbonate fuel cell for power generation. Thus, a major interest of this work is to adjust the applied current, volumetric flow rate, cell volume, residence time, and K_2CO_3 concentration, aimed at promoting CO_2 production from a CO_3^{2-}-containing solution in a basic electrochemical flow cell containing two metal plate electrodes separated by a cation exchange membrane. It is believed that such a work will complement the existing knowledge of electrochemistry-assisted carbon capture and enrichment including process design, proof of concept, thermodynamic analysis, techno-economic assessment, and reactive carbon separation.[11–26] Experimental results will be compared with a CO_3^{2-}-CO_2 model for the anode, providing more focus for the first time on both the electrochemical flow cell design and operation for reconditioning OH^--based facile CO_2 capture solvents in comparison of Ref. 11.

Experimental Methodology

Experimental process.—A process for investigating CO_2 release at the anode of an electrochemical flow cell is shown in Fig. 2. During testing, two MasterFlex L/S peristaltic pumps continued feeding the same 0.77 M or 0.37 M K_2CO_3 solution into the cathode and anode chambers from a holding tank at the flow rate of 10.4 or 4.1 ml min^{-1} for the anode and 8.6 ml min^{-1} for the cathode. In the anode chamber, OH^- was electrochemically consumed to produce O_2, which was real-time monitored by an inline Hanna pH probe at the anode outlet. Under such a scenario, the chemical equilibrium of CO_3^{2-} shifts to produce CO_2 in the anode chamber. To quantify both O_2 and CO_2, a custom gas-liquid separator was placed after the pH cell, where the gases were first separated from the solution by settling, followed immediately by mixing with N_2 as carrier gas prior to entering a sequence of a Thermo Fisher flow meter, an inline Neulog O_2 sensor, and a Horiba VIA-510 CO_2 analyzer, as highlighted in Fig. S1(available online at stacks.iop.org/JES/169/044527/mmedia). Another MasterFlex L/S peristaltic pump was used to stabilize the solution level in the gas-liquid separator. Finally, a solution sample from the separator was collected and

[z]E-mail: ayokunle.omosebi@uky.edu; kunlei.liu@uky.edu

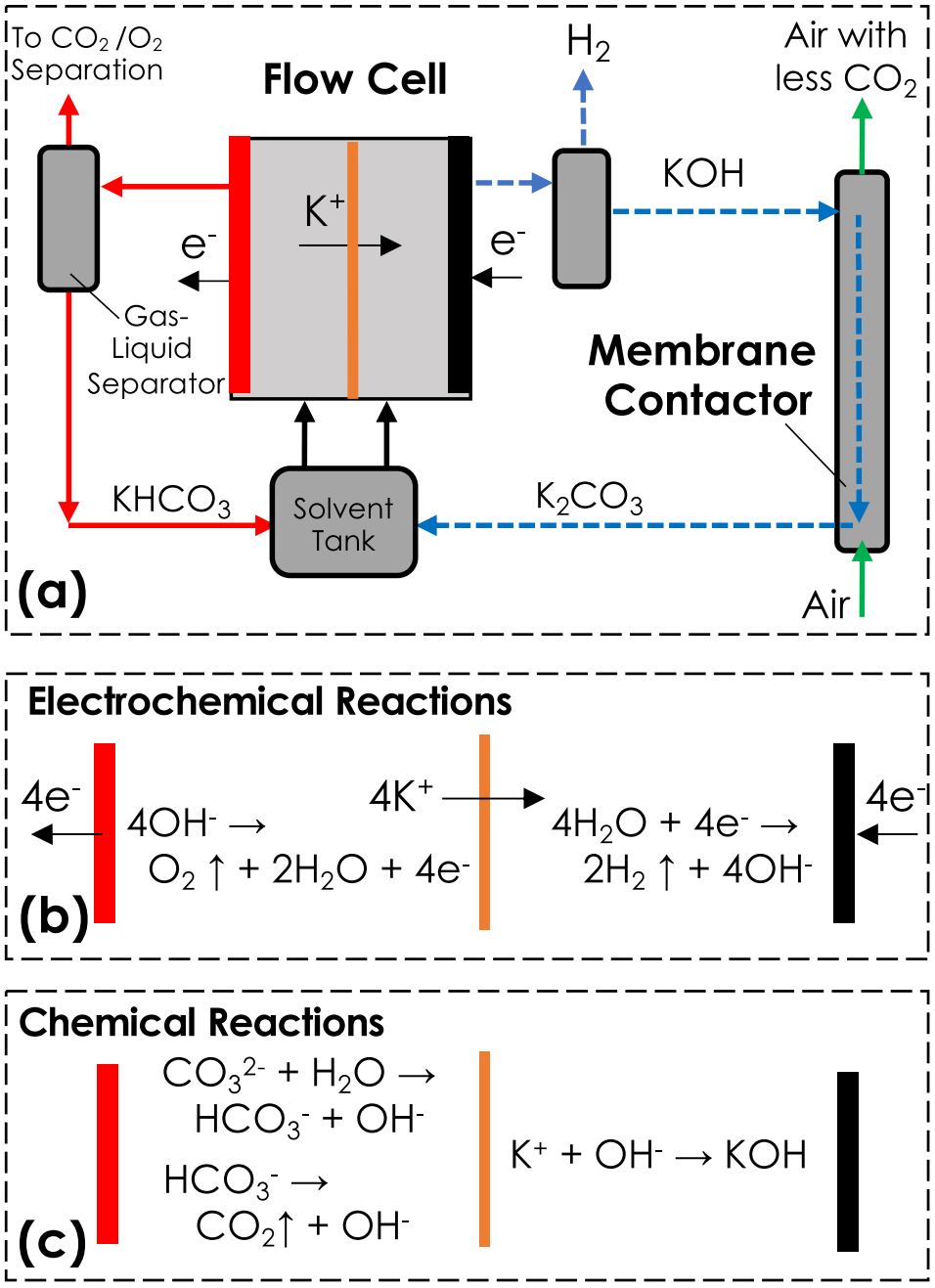

Figure 1. (a) A process sketch of a membrane-electrochemical CO_2 capture system featuring a membrane contactor for CO_2 capture and an electrochemical flow cell for solvent regeneration. (b) and (c) Demonstration of reactions in the electrochemical flow cell when the solvent is regenerated.

sealed in a high-density polyethylene (HDPE) bottle to later measure its total alkalinity. For the catholyte route, the configuration was like the anolyte route but without measuring H_2 and alkalinity. All the tests were conducted at 22 °C–25 °C. The setup photos, including a bench-scale DAC process and a custom gas-liquid separator, are provided in Fig. S1 with additional descriptions such as operating scenarios for the gas-liquid separator and calibration methods for the analyzer and sensors.

Electrochemical flow cell.—The electrochemical flow cell was equipped with a pair of 16 cm^2 annealed 316 stainless-steel plate electrodes separated by a Nafion 115 membrane. Since CO_2 release is the secondary reaction succeeded by the primary O_2 evolution at the anode, investigating the effect of the anode chamber volume and residence time on CO_2 release becomes the key interest in this work. To perform such a test, one method was to change the silicone rubber gasket that was laid between the membrane and each electrode. Consequently, the volume of the anode chamber could be varied by changing the gasket thickness, resulting in the different residence times.

Alkalinity measurement.—To measure changes in the concentration K^+ before and after water electrolysis, the total alkalinity of the solution collected from the anolyte route was measured at room temperature by acid titration using a Metrohm Titrando 836 automatic titrator. Such testing aims to explain the discrepancies between the experimental and modeled results for CO_2 release and pH reduction. During testing, approximately 1 g of the sample was continuously titrated with 0.08 M H_2SO_4 solution until its pH was 2.5. (See the typical titration curve from this study in Fig. S2.) The volume of the

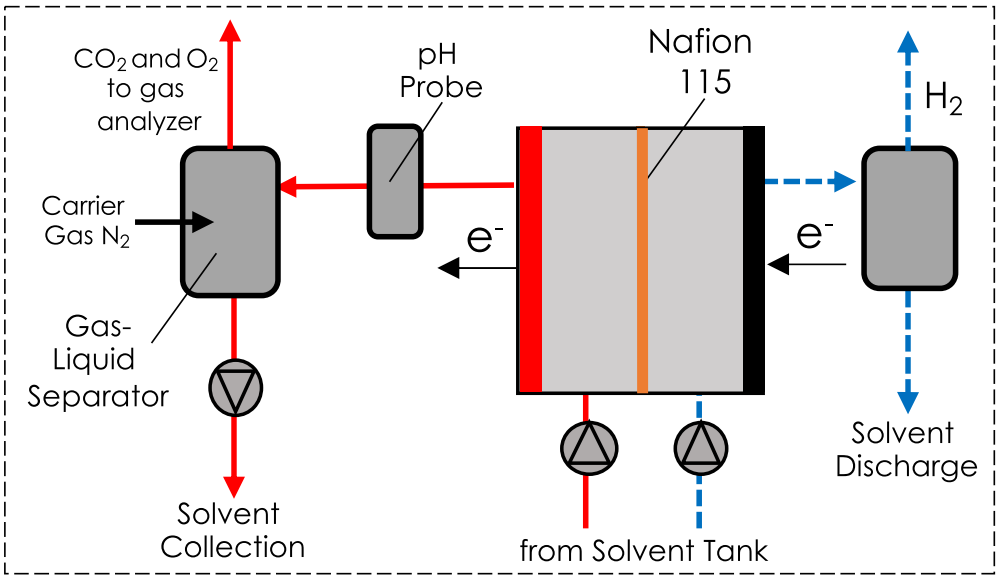

Figure 2. A process used to study CO_2 release at the anode of an electrochemical flow cell. A K_2CO_3 solution was continuously fed into the cell by two peristaltic pumps. In the anolyte route (solid red lines), both the solution's pH at the anode outlet and gas concentrations were measured in situ. The solution from the anode after the process was collected for the alkalinity analysis to quantify the concentration of K^+.

acid at the final equivalent point was used to calculate the total alkalinity of the sample. The standard deviation for repeating measurements was smaller than 1% in the present study. To convert the unit of mol kg^{-1} to mol l^{-1}, the density of each sample was measured at room temperature using a 10 ml glass volumetric flask with a Thermo Fisher digital balance with 4 decimal places.

Theoretical approach.—In a K_2CO_3 solution, reducing pH or OH^- of the solution makes CO_3^{2-} become CO_2 via

$$CO_3^{2-} + H_2O \leftrightarrow HCO_3^- + OH^- \quad [1]$$

$$HCO_3^- \leftrightarrow CO_2^* + OH^- \quad [2]$$

$$H_2O \leftrightarrow H^+ + OH^- \quad [3]$$

where CO_2^* in reaction 2 means dissolved CO_2 in the solution, which will be emitted from the solution to the atmosphere when the concentration or partial pressure of CO_2^* is greater than that in air according to Henry's law.[27] When reactions 1–3 are in equilibrium, their equilibrium constants, K_i , are expressed in terms of activity (estimated as concentration) values of the relevant species, such that

$$K_1 = [HCO_3^-][OH^-]/[CO_3^{2-}] \quad [4]$$

$$K_2 = [CO_2^*][OH^-]/[HCO_3^-] \quad [5]$$

$$K_3 = [H^+][OH^-] \quad [6]$$

To calculate concentration values for all the species in reactions 4–6, 2 more equations are needed, of which the total amount of dissolved inorganic carbon, C_T, is the sum of

$$C_T = [CO_2^*] + [HCO_3^-] + [CO_3^{2-}] \quad [7]$$

In addition, because of charge conservation of the solution, the positively charged species must equal the negatively charged species, and thus,

$$[H^+] + [K^+] = [OH^-] + [HCO_3^-] + 2[CO_3^{2-}] \quad [8]$$

Simultaneous solving Eqs. 4–8 will provide a numerical solution of each species at equilibrium if the initial K_2CO_3 concentration value is given.[28]

To release CO_2 from a K_2CO_3 solution in the anode chamber, the chemical equilibrium of reactions 1–3 must be disrupted by consuming OH^-. To describe the OH^- consumption under a once-through operating mode for an electrochemical flow cell, rates of reactions 1 and 2, r_1 and r_2, respectively, are defined as follows

$$r_1 = k_1([CO_3^{2-}]_{eq\_i} - ([OH^-]_{eq}[HCO_3^-]_{eq})/K_1) \quad [9]$$

$$r_2 = k_2([HCO_3^-]_{eq\_i} - ([OH^-]_{eq}[CO_2^*]_{eq})/K_2) \quad [10]$$

where k_1 and k_2 are the respective rate constants for reactions 1 and 2, and the subscript eq_i denotes the initial concentration value at equilibrium before water electrolysis begins, which is calculated via Eqs. 4–8. Since the volume of the anode chamber, V, is the product of the surface area of the anode with the thickness of the silicon rubber gasket, the effluent molar rate of the OH^- in the anode chamber, m_{OH^-}, at the steady-state water electrolysis is

$$m_{OH^-} = m_{OH^-,eq\_i} + (r_1 + r_2)V - n_{OH^-} \quad [11]$$

$$n_{OH^-} = i_{app}\beta_{eff}/F \quad [12]$$

where n_{OH^-} represents the molar rate of OH^- consumption for O_2 evolution, which is related to i_{app}, the current applied to the electrochemical flow cell, β_{eff}, the current utilization efficiency for K^+ across a cation-exchange membrane or the portion of electronic charge used to remove K^+ from the anode to cathode chamber, and, F, the Faraday constant. To convert the molar rate to concentration, both sides of Eq. 11 are divided by the volumetric flow rate of the solution, Q_{sol}, providing

$$[OH^-]_{eq} - [OH^-]_{eq\_i} = (r_1 + r_2)\tau - (i_{app}\beta_{eff})/(Q_{sol}F) \quad [13]$$

$$\tau = V/Q_{sol} \quad [14]$$

in which τ is the residence time of the solution at the anode. The $[OH^-]$ in Eq. 13 is used to refresh the concentration values for all the species in reactions 1–3 at a new equilibrium via Eqs. 4–8. Consequently, the deficiency of C_T before and after water electrolysis is the quantity of CO_2 release, as the $[CO_2^*]$ transformed from CO_3^{2-} will exceed the CO_2 partial pressure or solubility under Henry's law.

Equation 13 outlines that the applied current, residence time, volumetric flow rate, and anode chamber volume can affect OH^- (or pH) reduction toward CO_2 release, meaning that $[OH^-]_{eq\_i}$—$[OH^-]_{eq}$ is needed to become greater for more CO_2 release. For instance, the last term, $(i_{app}\beta_{eff})/(Q_{sol}F)$, from Eq. 13 suggests that the OH^- reduction can be enhanced by decreasing the volumetric flow rate, Q_{sol}, and/or increasing the current, i_{app}, thereby creating a lower pH environment to promote CO_2 release from a CO_3^{2-} solution via reactions 1 and 2. Similarly, the middle term, $(r_1 + r_2)\tau$, from Eq. 13, should be minimized. To reduce the residence time, as per Eq. 14, reducing the anode chamber volume, V, or increasing the volumetric flow rate, Q_{sol}, are the approaches; however, the latter approach alleviates the effectiveness of OH^- reduction due to the decrease in $(i_{app}\beta_{eff})/(Q_{sol}F)$, as opposed to decreasing the volumetric flow rate to enhance OH^- reduction as stated above.

Tests Development.—To validate the discussion regarding Eq. 13 for CO_2 release driven by OH^- reduction, 5 cases are specifically considered in Table I. Cases A versus B aims to study the effect of the volumetric flow rate on CO_2 release, as both cases are shared with a very close residence time, 20.8 and 20.5 s for cases A and B, respectively, thereby eliminating impacts of the residence time on CO_2 release coming from $(r_1 + r_2)\tau$ in Eq. 13. Cases B versus C (or versus E) focuses on the effectiveness of CO_2 release related to the residence time, in which the residence time is modified by only changing the volume of the anode chamber, removing the interference from the flow rate in the $(i_{app}\beta_{eff})/(Q_{sol}F)$ of Eq. 13. Moreover, the impact of the K_2CO_3 concentration on CO_2 release was investigated via cases C versus D.

All the cases were evaluated using the process in Fig. 2 with the electrochemical flow cell operated at a fixed i_{app} for 20 min under a once-through mode. To discuss the experimental results, the CO_2 release and pH reduction were modeled using the constants in Table II. Finally, unless noted elsewhere, the volume and volumetric flowrate for the cathode chamber were fixed at 3.6 ml and 8.6 ml min^{-1}, respectively.

Results and Discussion

Typical process.—Typical cell responses in terms of the cell voltage, pH at the anode outlet, and gas concentrations are displayed in Fig. 3 as a function of testing time. In Fig. 3a, increasing i_{app} increases the cell voltage, whereas the steady-state anode pH decreases. Since the cell voltage is much greater than the thermodynamic voltage for water splitting, OH^- is very likely to be converted to O_2 via $4OH^- \rightarrow O_2\uparrow + 2H_2O + 4e^-$, while acidifying the K_2CO_3 solution in the anode chamber to release CO_2. Thus, in Fig. 3b, both the O_2 and CO_2 concentrations increase by increasing i_{app}. By applying the same step current charging technique, the other cases in Table I were tested, and the relevant process data like Fig. 3 are shown in Fig. S3.

To facilitate further discussion, the experimental values of gas evolutions and pH at steady state are extracted from the process data and then averaged for analysis. For instance, the averaged gas concentration in vol%, C_{vol}, is converted to its equivalent current, $i_{CO_2\ (or\ O_2)}$, in Amps by assuming 25 °C and 1 atm via

$$i_{CO_2\ (or\ O_2)} = \alpha C_{vol} Q_{gas} n \quad [15]$$

where α is the constant stemmed from the calculations regarding Fig. S5, Q_{gas} is the gas flow rate measured by the flow meter, and n is the number of electron transfer, 2 for CO_2 and 4 for O_2 as per $CO_3^{2-} + H_2O \leftrightarrow HCO_3^- + OH^-$, $HCO_3^- \leftrightarrow CO_2\uparrow + OH^-$, and $4OH^- \rightarrow O_2\uparrow + 2H_2O + 4e^-$. Consequently, the current efficiency is defined as the ratio of the equivalent current to applied current such as i_{CO_2}/i_{app} for CO_2 release and i_{O_2}/i_{app} for O_2 evolution.

Case-by-case comparisons.—The experimental i_{CO_2}/i_{app} and pH curves are plotted in Figs. 4a and 4b, respectively, as a function of i_{app}. All the cases exhibit increases in the CO_2 production and decreases in the pH by increasing the i_{app}; however, unlike O_2 evolution with a consistent i_{O_2}/i_{app} value of ~0.9 for all the cases, independent of the i_{app} in Fig. S5, the behavior of the i_{CO_2}/i_{app} (and pH reduction) depends significantly upon the flow rate, cell volume, and K_2CO_3 concentration associated with the anode of the electrochemical flow cell.

As shown in case A with the higher volumetric flow rate versus case B with the lower volumetric flow rate, reducing the volumetric flow rate substantially benefits CO_2 release as i_{app} increases, e.g., for case B, the i_{CO_2}/i_{app} increases from 0.03 at 4 A to 0.21 at 7 A; in contrast, the i_{CO_2}/i_{app} for case A is much smaller, with only 0.001 at 4 A and 0.005 at 7 A. Such i_{CO_2}/i_{app} responses agree with the pH reduction associated with cases A and B in Fig. 4b, e.g., from 4 to 7 A, the pH for cases B and A drops by 1.9 and 0.3, respectively. In Figs. 4c and 4d, both the modeled i_{CO_2}/i_{app} and pH curves present similar trends to the respective results from the experiments, showing the much more pronounced CO_2 release and pH reduction for case B than that for case A. Since cases A and B have similar residence time of about 20 s, the significant improvement of CO_2 release is accounted for by increasing the $(i_{app}\beta_{eff})/(Q_{sol}F)$ in Eq. 13 or ratio of i_{app} to Q_{sol}, with the implication that reducing the flow rate can substantially enhance the effectiveness of OH^- reduction per volume unit of K_2CO_3 solution when a fixed current is applied.

The effect of residence time on CO_2 release and pH is also captured in Figs. 4a and 4b, respectively. Herein, the residence time is modified by only changing the volume of the anode chamber to

Table I. Testing conditions were used to release CO_2 from a K_2CO_3 solution. The electrochemical flow cell was charged at 2–7 A and at room temperature. Please note that volume and volumetric flowrate for the cathode chamber were fixed at 3.6 ml and 8.6 ml min^{-1}, respectively, in this work.

Case	Testing Conditions			
	Anode volume/ml	Anode flowrate/ml min^{-1}	Residence time/s	K_2CO_3 Conc/M
A	3.6	10.4	20.8	0.77
B	1.4	4.1	20.5	0.77
C	3.6	4.1	52.7	0.77
D	3.6	4.1	52.7	0.37
E	14.4	4.1	210.8	0.77

Table II. The constants used to model CO_2 release and pH reduction at 25 °C. Please note that the β_{eff} was selected at 0.5, 0.75, and 1 to discuss the discrepancy between the experimental and modeled results.

Parameter	Value	References
K1/M-1	10–3.67	28
K2/M-1	10–7.65	28
K3/M-1	10–14	28
k1/s-1	3.06 × 105	29
k2/s-1	9.71 × 10–5	29
F/C mol-1	96,485	30
Ceff	0.5, 0.75, and 1	N/A

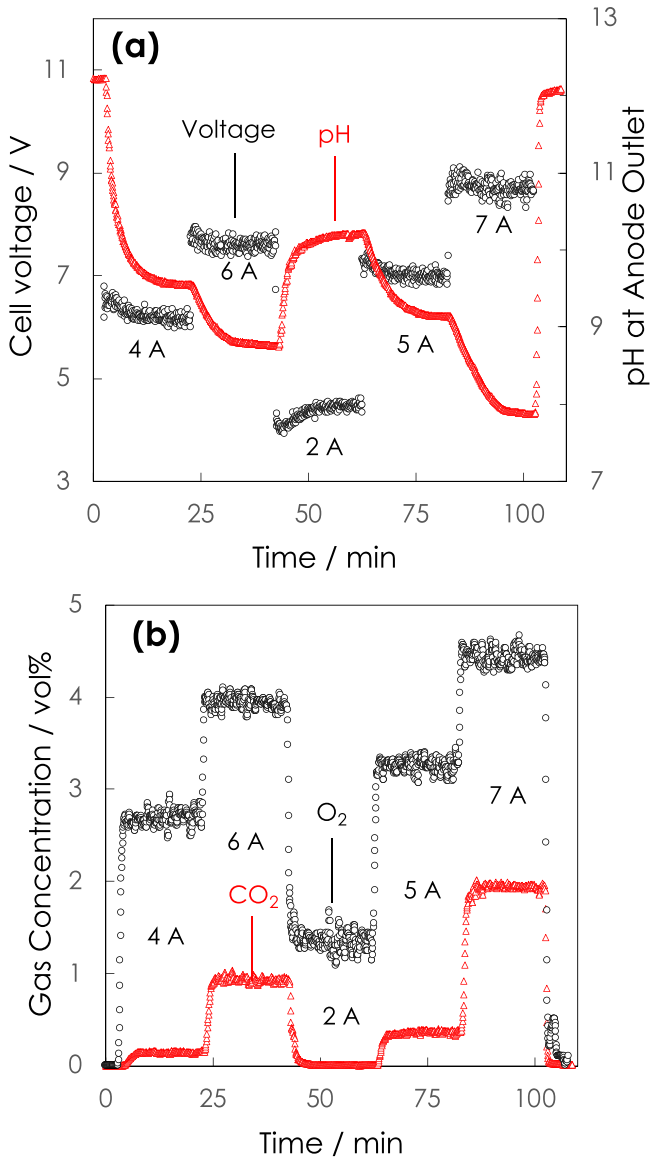

Figure 3. Process data from case C is used to illustrate the typical cell responses under the step current charging, including (a) voltage and pH and (b) O_2 and CO_2 concentrations as a function of testing time.

diminish interference of the flow rate as per Eq. 14. Under the same flow rate, case B with the shorter residence time (or smaller anode volume) versus case C (or E) with the longer residence time (or larger anode volume) depicts comparable i_{app} utilization on CO_2 release and pH reduction, e.g., for case C, the i_{CO_2}/i_{app} increases from 0.02 at 4 A to 0.19 at 7 A, marginally lower than the values for case B with 0.03 at 4 A to 0.21 at 7 A. The modeled results show very similar behavior of i_{CO_2}/i_{app} and pH for both the cases as shown in Figs. 4c and 4d, in which the i_{CO_2}/i_{app} and pH curves for cases B, C, and E are nearly overlaid. Overall, both the experimental and modeled results express residence time (affected by the volume of the anode chamber) as a weak variable for controlling CO_2 release and pH reduction from a CO_3^{2-}-containing solution, likely due to the comparatively small rate constant for HCO_3^- consumption in Eq. 10. (Figure S6 shows that the differences of i_{CO_2}/i_{app} and pH between cases B and C will become great if the rate constants are changed.)

To study the effect of K_2CO_3 concentration on CO_2 release, cases C and D with the same flow rate and residence time are compared. In Figs. 4a and 4b, in contrast to case C with the higher K_2CO_3 concentration, case D with the lower K_2CO_3 concentration performs remarkably for CO_2 release and pH reduction, e.g., at 4 A, i_{CO_2}/i_{app} is 0.24 at pH of 7.2 for case D versus i_{CO_2}/i_{app} is 0.02 at a pH of 9.5 for case C. Such a considerable difference is also clearly reflected by modeling the i_{CO_2}/i_{app} and pH reduction for the two cases in Figs. 4c and 4d, respectively. The improved i_{CO_2}/i_{app} at the lower K_2CO_3 concentration is attributed to the reduced initial $[OH^-]_{eq\_i}$ in Eq. 13. However, excessively lowering the K_2CO_3 concentration will adversely affect cell operation by dramatically increasing cell voltage and energy consumption for CO_2 release, as shown in Figures S3 and S7.

Using the present cell architecture (two metal plate electrodes separated by a cation exchange membrane) possesses a significant energy cost in terms of CO_2 release in Fig. S7, which is much higher than 200–400 kJ $mol^{-1}CO_2$ reported in the contemporary literature.[12,13] Furthermore, if CO_2-O_2 mixture utilization in an MCFC or similar is not desired, energy will be spent on upgrading the CO_2 from the CO_2-O_2 mixture. To resolve such issues, both the cell architecture and process can be redesigned to use the H_2 produced at the cathode to feed the anode. Under such a scenario, it is believed that the cell operating voltage will be minimized via H_2 assisted anode depolarization while improving the pH reduction to facilitate CO_2 release.[12,31]

Through the case-by-case comparisons, the experimental results reveal that decreasing the anode's flow rate and/or K_2CO_3 concentration are the most influential ways for promoting CO_2 release. The same conclusion can be deduced by modeling the i_{CO_2}/i_{app} and pH reduction. However, discrepancies between the experimental and modeled values are observed, especially when i_{app} becomes significant (Fig. 4). Therefore, cases C and D are further used to elucidate possible causes of such discrepancies by adjusting β_{eff} in the model accompanied with the respective alkalinity values of the solutions collected from the anode.

H^+ Crossover causing decreases in β_{eff}.—Fig. 5 shows the modeled i_{CO_2}/i_{app} and pH reduction curves for cases C and D when β_{eff} is adjusted to 1, 0.75, and 0.5, combined with the relevant experimental data points. By evaluating the modeled curves at a fixed current, reducing the β_{eff} diminishes both the effectiveness of CO_2 release and pH reduction, e.g., at 6 A, the i_{CO_2}/i_{app} in Fig. 5a decreases from 0.5 at the $\beta_{eff} = 1$ to a negligible value at the $\beta_{eff} = 0.5$. It is also found that for both the cases, with increasing the i_{app}, the experimental data points gradually drift from one modeled curve with the higher β_{eff} to another with the lower β_{eff}, e.g., in Fig. 5b, the pH at 2–4 A is near the modeled curve with the $\beta_{eff} = 1$ versus the pH at 6–7 A is close to the modeled curve with the $\beta_{eff} = 0.75$. Such an observation suggests that even under the testing conditions with the same volumetric flow rate and K_2CO_3 concentration, the β_{eff} is perhaps current dependent, becoming smaller as the i_{app} gets larger.

Since H^+ is also available in the system via Eq. 6, in equilibrium with OH^-, the current-dependent loss of β_{eff} is likely due to H^+

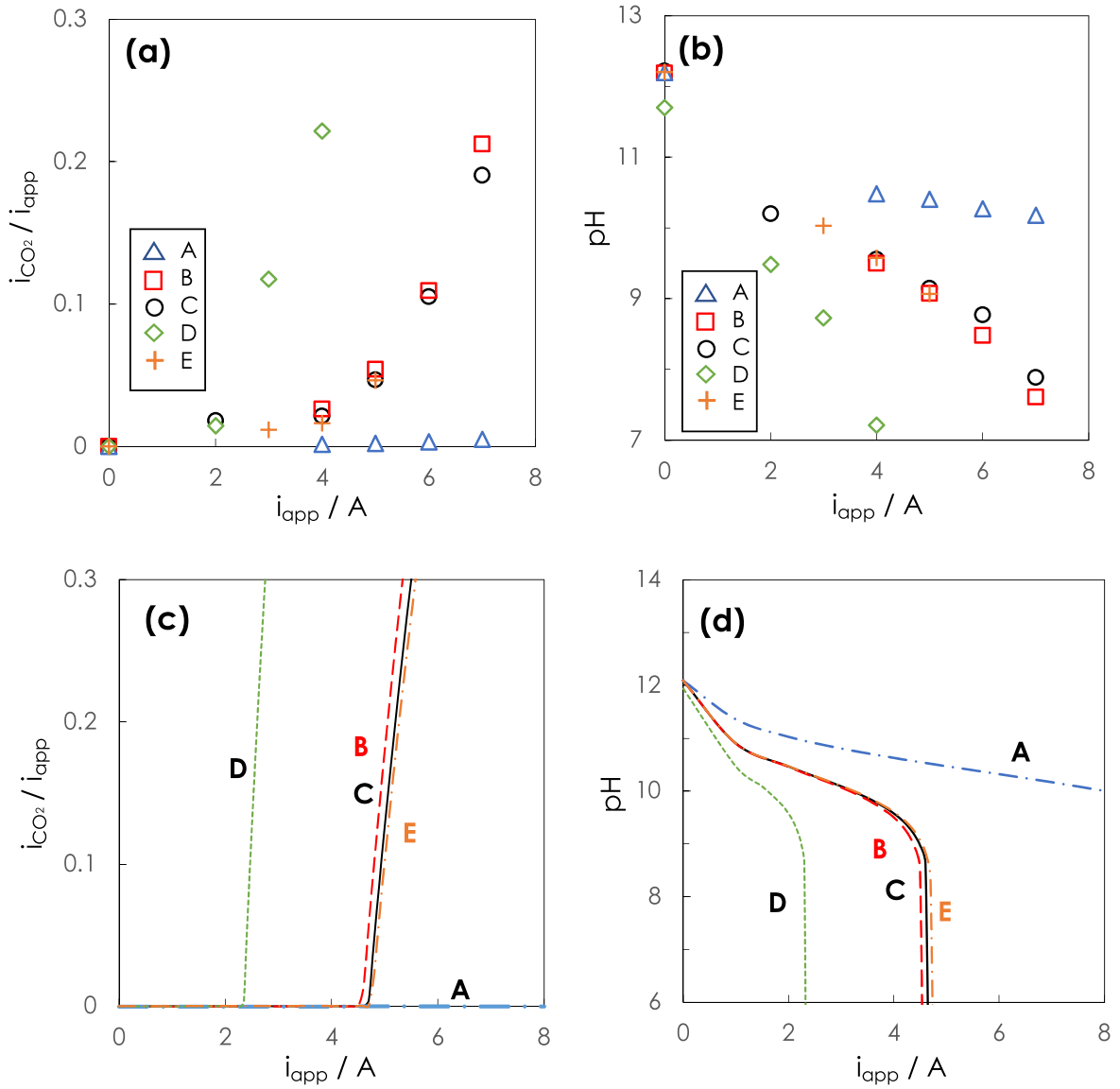

Figure 4. Comparison of (a) experimental i_{CO_2}/i_{app}, (b) experimental pH, (c) modeled i_{CO_2}/i_{app}, and (d) modeled pH as a function of i_{app} for all the cases. The modeled curves in (c) and (d) are plotted when β_{eff} is 1. The steady-state values from the process data for cases A-E are extracted from Figs. 3 and S4.

crossing the Nafion membrane during water electrolysis. To verify this hypothesis, the total alkalinity values of the K_2CO_3 solutions collected from the anode chamber were analyzed. Generally, alkalinity is the ionic charge difference between the conservative cations and anions unaffected by changing pH.[32] Therefore, as per Eq. 8, the alkalinity value in Table III is the same as the K^+ concentration value, which is utilized to calculate the K^+ equivalent current, i_{K^+}, via

$$i_{K^+} = \gamma(A_{T\_S} - A_{T\_i_{app}}) \quad [16]$$

where A_{T_S} is the alkalinity value for the starting solution, $A_{T\_i_{app}}$ is the alkalinity value for the solution collected at the i_{app}, and γ in the equation is determined based upon the solution's flow rate and Faraday constant. (See the supplementary information for details.) Moreover, to illustrate the H^+ crossover, the OH^- equivalent current, i_{OH^-}, is calculated using Eq. 15, the same procedure that has been used to calculate the i_{O_2} according to $4OH^- \rightarrow O_2\uparrow + 2H_2O + 4e^-$. Finally, to facilitate the comparison, both the i_{K^+} and i_{OH^-} are normalized by i_{app}, and the relevant results are in the two last columns of Table III.

As illustrated previously in Fig. 1, the number of the K^+ repulsed from the anode to cathode chambers ideally equals the number of the OH^- consumed for O_2 evolution, meaning that both the values of i_{K^+}/i_{app} and i_{OH^-}/i_{app} should be the same at a fixed i_{app}. In fact, in Table III, the i_{K^+}/i_{app} is smaller than the i_{OH^-}/i_{app} at every i_{app}, suggesting that H^+ coming from H_2O dissociation via reaction 3 may substitute for the K^+ charge transferred across the membrane. Since H^+ has a smaller size than K^+,[33] in addition to a Nafion membrane with less cation selectivity,[34] removing H^+ from the anode may become facile at elevated i_{app}. If i_{app} increases, H_2O dissociation will also be intensified to enhance H^+ production, as more OH^- is consumed toward O_2 evolution. Consequently, more H^+ will migrate across the membrane along with K^+, therefore continuously differentiating the experimental and modeled results in Fig. 5.

Insights from continuous DAC operation.—Additional work is conducted for continuous DAC operation by using the setup depicted in Fig. S1a, where the flow cell is used for solvent generation and the membrane contactor is used for carbon capture. As shown in Fig. 6a, increases in pH of the solvent improve the effectiveness of capturing CO_2 from the atmosphere. For example, at the first testing period by

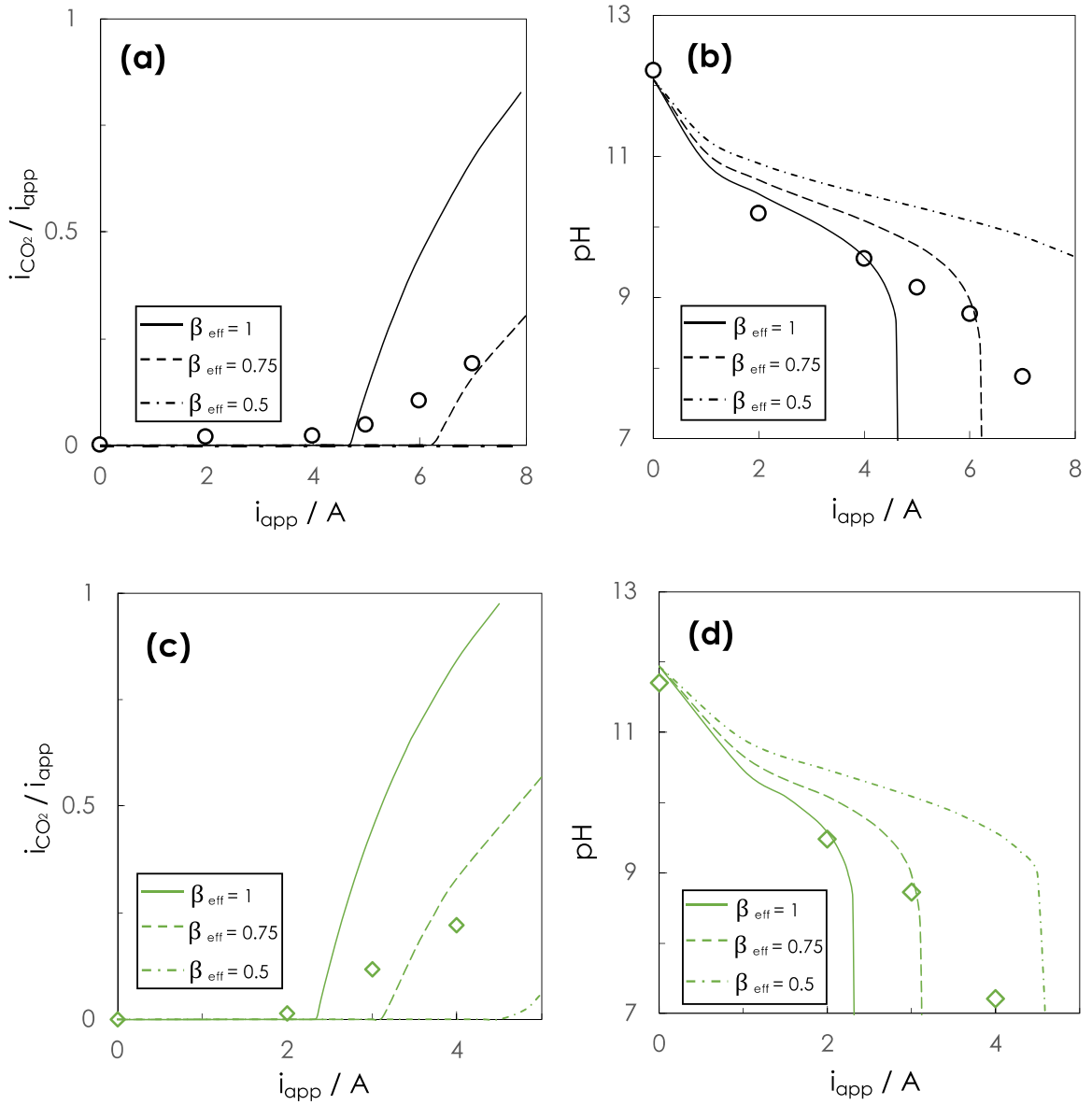

Figure 5. Comparison of the experimental and modeled results for the i_{CO_2}/i_{app} and pH reduction by adjusting β_{eff}, in which plots (a) and (b) belong to case C, and plots (c) and (d) are affiliated with case D. The other constants like rate and equilibrium constants are listed in Table II.

Table III. Using the total alkalinity values to calculate the i_{K^+}/i_{app} for cases C and D. Each sample was measured 3 times. The value in the bracket shows the standard deviation.

Case	K_2CO_3 sample collected at i_{app}	Alkalinity/mol L^{-1}	i_{K^+}/i_{app}	i_{OH^-}/i_{app}
C	Starting	1.550 (0.004)	N/A	
	2	1.265 (0.002)	0.94	0.94
	4	1.038 (0.002)	0.85	0.90
	5	0.924 (0.003)	0.83	0.91
	6	0.818 (0.001)	0.81	0.93
	7	0.713 (0.007)	0.79	0.91
D	Starting	0.742 (0.003)	N/A	
	2	0.468 (0.004)	0.91	0.89
	3	0.379 (0.002)	0.80	0.89
	4	0.281 (0.003)	0.77	0.88

400 min, when the pH is varied between 12.8 and 13.3, the remaining CO_2 concentration in the treated air is approximately 150 ppm, corresponding to about 63% instant CO_2 capture rate; in contrast, during the final testing stage after 1,350 min, when the pH increases to 13.6–13.8, the remaining CO_2 concentration decreases to about 90 ppm. The improved CO_2 capture is mainly accounted for by the OH^- production at the cathode, as discussed in the introduction. Moreover, from the process, the H_2 formed at the

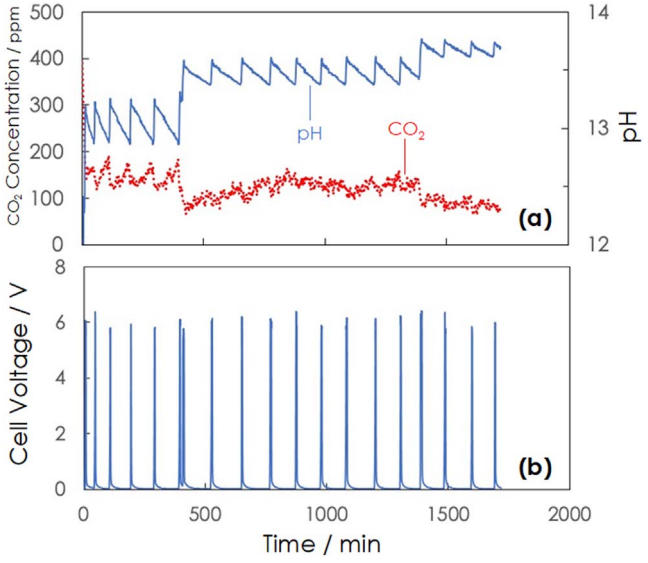

Figure 6. A continuous direct air capture (DAC) process using the setup depicted in Fig. S1(a). (a) CO_2 concentration and pH of carbon capture solvent and (b) cell operating voltage for solvent regeneration as a function of testing time. The sawtooth pattern of pH in (a) is caused by the intermittent solvent regeneration at the cathode through the process. The solvent regeneration was controlled by a relay that was slaved to a pH sensor in the holding tank for the membrane contactor. When the pH was lower than the set point, the relay switch closed, triggering the power supply to charge the flow cell at the desired current. Therefore, a repaid increase in the cell voltage is observed in (b) while increasing the pH in (a). The experimental condition includes: the air flow rate was 1 L min^{-1}, the starting solvent was about 500 g of 6.7 wt% K_2CO_3 solution, the flow rate of the anode was 16 ml min^{-1}, the flow rate of the cathode was 50 ml min^{-1}, and the applied current was 1.5 A.

cathode can be beneficially utilized, e.g., reducing the cell operating voltage via depolarization by feeding H_2 to the anode, and therefore offsetting the operating cost of DAC.

To make the process sustainable, the captured CO_2 as CO_3^{2-} should be liberated at the anode by lowering the pH of the anolyte, which is driven by water electrolysis. However, it is found that under these experimental conditions (See the caption of Fig. 6), especially at a high flow rate for the anode and a low applied current, pH of the anolyte, the liquid in the anode chamber, is not reduced greatly for CO_2 release. For this case, pH of the anolyte sample (collected during the 1.5 A charging) was about 10.2, and no significant changes in the carbon loading were found.

This continuous DAC operation leads to two major conclusions: (1) to attain a high CO_2 capture rate, KOH needs to be continuously supplied to a membrane contactor via water electrolysis from the cathode of an electrochemical flow cell; and (2) imbalanced CO_2 capture and CO_2 release will occur in the present setup if operating conditions are improper, e.g., high flow rate and low applied current. Moreover, if attaining a high CO_2 capture rate is unnecessary, HCO_3^- will be produced from CO_2 reacting with CO_3^{2-}. Under such an operating condition, CO_2 release at the anode will be improved as more HCO_3^- coexists in the solvent.

Conclusions

In this study, a membrane-electrochemical CO_2 capture-enrichment process for DAC is demonstrated, focusing on elucidating the CO_2 release versus O_2 evolution from a CO_3^{2-}-solution at the anode of an electrochemical flow cell during water electrolysis. Through the case-by-case comparisons coupled with the modeled results, lowering the flow rate, reducing CO_3^{2-} concentration and increasing current are the effective methods to enhance CO_2 release, whereas changing the residence time and anode chamber volume offers minor effects. For instance, from case A versus case B, ~2.5 × reduction in the flow rate results in ~20 × increase in CO_2 release at 4 A, and in contrast, from case B versus case E, increasing the residence time by ~10 folds shows no improvement of CO_2 release. Moreover, discrepancies of the CO_2 release and pH reduction between the experimental and modeled results may be caused by H^+ crossover rather than K^+ transport through the Nafion membrane during water electrolysis.

Acknowledgments

These authors are very grateful for the research opportunity from the U.S. Department of Energy under the agreements of DE-FE0031962 and DE-FE0032125.

ORCID

Xin Gao https://orcid.org/0000-0002-8865-1697

References

1. https://unfccc.int/process-and-meetings/the-paris-agreement/the-paris-agreement, last access on 4-21-2022.
2. G. T. Rochelle, *Science*, **325**, 1652 (2009).
3. R. R. Bottoms, "Process for separating acidic gases." *in United States Patent Office*, ed. G. Corp (Girdler Corp, USA) (1930).
4. R. A. Frimpong, H. Nikolic, D. Bahr, G. Kiran, and K. Liu, *Int. J. Greenh. Gas Con.*, **106**, 103290 (2021).
5. R. W. Baker, B. Freeman, J. Kniep, Y. I. Huang, and T. C. Merkel, *Ind. Eng. Chem. Res.*, **57**, 15963 (2018).
6. https://netl.doe.gov/coal/carbon-capture/post-combustion, last access on 4-21-2022.
7. R. Socolow, M. Desmond, R. Aines, J. Blackstock, O. Bolland, T. Kaarsberg, N. Lewis, M. Mazzotti, A. Pfeffer, and K. Sawyer, *Direct air capture of CO_2 with chemicals: a technology assessment for the APS Panel on Public Affairs, in, American Physical Society*, (2011), https://aps.org/policy/reports/assessments/dac-biblio.cfm, last access on 4-21-2022.
8. R. Baciocchi, G. Storti, and M. Mazzotti, *Chem. Eng. Process.*, **45**, 1047 (2006).
9. D. W. Keith, G. Holmes, D. S. Angelo, and K. Heidel, *Joule*, **2**, 1573 (2018).
10. R. Sharifian, R. Wagterveld, I. Digdaya, C. Xiang, and D. Vermaas, *Energy Environ. Sci.*, **14**, 781 (2021).
11. S. Stucki, A. Schuler, and M. Constantinescu, *Int. J. Hydrog. Energy*, **20**, 653 (1995).
12. Q. Shu, L. Legrand, P. Kuntke, M. Tedesco, and H. V. M. Hamelers, *Environ. Sci. Tech.*, **54**, 8990 (2020).
13. F. Sabatino, M. Mehta, A. Grimm, M. Gazzani, F. Gallucci, G. J. Kramer, and M. van Sint Annaland, *Ind. Eng. Chem. Res.*, **59**, 7007 (2020).
14. S. E. Renfrew, D. E. Starr, and P. Strasser, *ACS Catal.*, **10**, 13058 (2020).
15. H. W. Pennline, E. J. Granite, D. R. Luebke, J. R. Kitchin, J. Landon, and L. M. Weiland, *Fuel*, **89**, 1307 (2010).
16. R. J. Gilliam, B. K. Boggs, V. Decker, M. A. Kostowskyj, S. Gorer, T. A. Albrecht, J. D. Way, D. W. Kirk, and A. J. Bard, *J. Electro. Soc.*, **159**, B627 (2012).
17. H. Nagasawa, A. Yamasaki, A. Iizuka, K. Kumagai, and Y. Yanagisawa, *AIChE J.*, **55**, 3286 (2009).
18. A. Iizuka, K. Hashimoto, H. Nagasawa, K. Kumagai, Y. Yanagisawa, and A. Yamasaki, *Sep. Purif. Tech.*, **101**, 49 (2012).
19. M. D. Eisaman, L. Alvarado, D. Larner, P. Wang, B. Garg, and K. A. Littau, *Energy Environ. Sci.*, **4**, 1319 (2011).
20. M. D. Eisaman, K. Parajuly, A. Tuganov, C. Eldershaw, N. Chang, and K. A. Littau, *Energy Environ. Sci.*, **5**, 7346 (2012).
21. G. H. Rau, *Environ. Sci. Tech.*, **42**, 8935 (2008).
22. J. H. Rheinhardt, P. Singh, P. Tarakeshwar, and D. A. Buttry, *ACS Energy Lett.*, **2**, 454 (2017).
23. I. A. Digdaya, I. Sullivan, M. Lin, L. Han, W.-H. Cheng, H. A. Atwater, and C. Xiang, *Nat. Commun.*, **11**, 1 (2020).
24. R. A. Shaw and T. A. Hatton, *Int. J. Greenh. Gas Con.*, **95**, 102878 (2020).
25. M. Wang and T. A. Hatton, *Ind. Eng. Chem. Res.*, **59**, 10120 (2020).
26. B. Gurkan, X. Su, A. Klemm, Y. Kim, S. M. Sharada, A. Rodriguez-Katakura, and K. J. Kron, *Iscience*, **24**, 103422 (2021).
27. W. Henry, *Philosophical Transactions of the Royal Society of London*, **93**, 29 (1803).
28. S. K. Lower, *Carbonate equilibria in natural waters* (1999), https://chem1.com/acad/webtext/pdf/c3carb.pdf, last access on 4-21-2022.
29. K. G. Schulz, U. Riebesell, B. Rost, S. Thoms, and R. E. Zeebe, *Mar. Chem.*, **100**, 53 (2006).
30. A. J. Bard and L. R. Faulkner, *Electrochemical Methods: Fundamentals and Applications, 2nd Edition* (Wiley, New York) (2000).
31. T. Mokkelbost, O. Kjos, O. Paulsen, B. Øye, H. Gudbrandsen, A. P. Ratvik, and G. M. Haarberg, *Light Metals 2014* 765(Springer, Berlin) (2014).
32. Aqion, The Concept of Alkalinity, in, Aqion.de, last access on 4-21-2022.
33. J. N. Israelachvili, *Intermolecular and Surface Forces* Third Edition ed., ed. J. N. Israelachvili 71(Academic, San Diego New York) (2011).
34. W. Y. Hsu and T. D. Gierke, *J. Membrane Sci.*, **13**, 307 (1983).